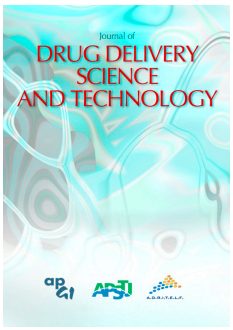

Cephalexin loading and controlled release studies on mesoporous silica functionalized with amino groups

Kiara Montiel-Centeno, Deicy Barrera, Fátima García-Villén, Rita Sánchez-Espejo, Ana Borrego-Sánchez, Enrique Rodríguez-Castellón, Giuseppina Sandri, César Viseras, Karim Sapag

PII: S1773-2247(22)00258-1

DOI: https://doi.org/10.1016/j.jddst.2022.103348

Reference: JDDST 103348

To appear in: *Journal of Drug Delivery Science and Technology*

Received Date: 29 November 2021

Revised Date: 11 April 2022

Accepted Date: 16 April 2022

Please cite this article as: K. Montiel-Centeno, D. Barrera, Fá. García-Villén, R. Sánchez-Espejo, A. Borrego-Sánchez, E. Rodríguez-Castellón, G. Sandri, Cé. Viseras, K. Sapag, Cephalexin loading and controlled release studies on mesoporous silica functionalized with amino groups, *Journal of Drug Delivery Science and Technology* (2022), doi: https://doi.org/10.1016/j.jddst.2022.103348.

Author Statement

The authors confirm contribution to the paper as follows: **Conceptualization, methodology, validation and formal analysis:** K. M-C., D. B., F. G-V., R. S-E., A. B-S., E. R-C., G. S., C. V., K. S. **Investigation:** K. M-C., D. B., F. G-V., R. S-E., A. B-S., E. R-C., G. S. **Resources:** E. R-C., G. S., C. V., K. S. **Data curation:** K. M-C. **Writing-original draft:** K. M-C. **Writing-review & editing:** D. B., F. G-V., R. S-E., A. B-S., E. R-C., C. V., K. S. **Visualization:** D. B., F. G-V., C. V., K. S. **Supervision, project administration and funding acquisition:** C. V., K. S. All authors have read and agreed to the published version of the manuscript.

Cephalexin loading and controlled release studies on mesoporous silica functionalized with amino groups

Kiara Montiel-Centeno[a,b], Deicy Barrera[a], Fátima García-Villén[b], Rita Sánchez-Espejo[b], Ana Borrego-Sánchez[b], Enrique Rodríguez-Castellón[c], Giuseppina Sandri[d] César Viseras[b,e*], Karim Sapag[a*]

[a.] *Laboratorio de Sólidos Porosos. Instituto de Física Aplicada. CONICET. Universidad Nacional de San Luis. Ejército de los Andes 950. CP: 5700 – San Luis. Argentina.*

[b.] *Deparment of Pharmacy and Pharmaceutical Technology, University of Granada, 18071 Granada, Spain.*

[c.] *Departamento de Química Inorgánica, Unidad Asociada al Instituto de Catálisis (CSIC), Facultad de Ciencias, Universidad de Málaga, 29071 Málaga, España.*

[d.] *Deparment of Drug Sciences, University of Pavia, viale Tatamelli 12, 22100 Pavia, Italy.*

[e.] *Andalusian Institute of Earth Sciences (Consejo Superior de Investigaciones Científicas-University of Granada) Armilla, 18100 Granada, Spain.*

Abstract

KIT-6 mesoporous silica has been synthesized using the sol-gel method and functionalized with 3-aminopropyl triethoxysilane by grafting route to obtain KIT-6/NH_2. These samples were used as carriers in the loading and controlled release of cephalexin (CFX). The effect of temperature and gastric and intestinal pH on the stability of pure CFX and loaded in KIT-6 and KIT-6/NH_2 were investigated. The properties of the synthesized materials and their CFX loading capacity were studied through FTIR, ads-des N_2 at 77 K, TEM, SEM, XPS, and TGA. The controlled release tests were carried out in a simulated physiological medium at gastric (1.2) and intestinal pH (6.8). Furthermore, the biocompatibility of both materials was studied through cell viability tests in Caco-2 intestinal cells. The results revealed that KIT-6 and KIT-6/NH_2 had similar CFX loading capacities. It was found that CFX degrades at pH 6.8, however, KIT-6 and KIT-6/NH_2 were able to protect it from the aforementioned degradation. Moreover, KIT-6 materials presented a good performance as CFX carriers since both materials provided diffusion-controlled release profiles during 24 h, satisfying the

Korsmeyer-Peppas kinetic model. Mesoporous silicas presented in this work are promising candidates to be used in CFX controlled release systems due to their chemical interactions, textural properties, and high cell viability.

Keywords: Cephalexin, drug delivery system, functionalization, KIT-6, loading, release.

* Corresponding author: cviseras@ugr.es (C.V); sapag@unsl.edu.ar (K.S)

1. Introduction

Mesoporous silica materials (MSM) have received increasing attention due to their outstanding features: high specific surface area, large pore volume, tunable pore size, ordered pore distribution, rigid inorganic structure, and low toxicity, biocompatibility, and functional surface [1–4]. These attractive features have made MSM widely used in different scientific and technological areas such as catalysis, adsorption, and biomedicine, among others [5–7]. Compared to conventional dosage forms, modified drug delivery systems (MDDS) intend to improve the bioavailability of drugs and minimize adverse effects by changing the rate and time of drug release. The aim of using an MDDS is to transport the active(s) substance(s) towards a specific site of the organism where it will be released in a controlled manner to guarantee maximum bioavailability with minimum side effects [8,9].

As MDDS excipients, MSM has received much attention due to their unique features previously described. The high surface area provides enough space for drug interactions and potentially high drug loading capacity. The large pore volume allows the hosting of therapeutic molecules with a wide variety of molecular sizes. The ordered porosity and the narrow pore size distribution are of great interest in drug delivery control, favoring the diffusion of the adsorbed drugs in a controlled way with high reproducibility of the results [10]. Additionally, the rigid inorganic structure of MSM provided them with

outstanding resistance to environmental stressors, such as pH, hydrolysis, heat, and mechanical stress. The MSM are currently considered low toxicity materials and have received "Generally Recognized As Safe" status by the United States Food and Drug Administration (US FDA GRAS report) [11]. However, more reports on biocompatibility are still needed to ensure adequate safety since each material complexity must be considered, which differ substantially in the surface chemistry, the particle size, and the possible presence of solvents or suspending media [11].

The surface of MSM consists of silanol groups that can interact with different molecules through different mechanisms depending on the pH and functional groups of the molecules at stake [12]. Nonetheless, not all the drugs can interact with silanols groups, and in some cases, the interactions are weak, which does not allow controlled release profiles. Thus, results of great interest the surface functionalization of MSM by anchoring chemical groups allowing stronger interactions. Functionalization is carried out to add additional molecules to the surface of the MSM, modifying their surface properties and the nature of the interactions between MSM and active substances. Optimal MSM functionalizations have been reported to improve drug loading capacity and release control [4,13,14].

Several studies on the development of MSM-drug delivery systems have been previously published. Ayad *et al*. [15] explored the synthesis and amine functionalization of mesoporous silica KIT-6 using as carriers of ketoprofen and 5-fluorouracil. These authors found that the loading capacity and the release behavior depend on the textural properties of the silica (pore size and surface area). The same conclusion was reached by Latifi and Sohrabnezhad [16], who used KIT-6 and MCM-41 with and without amine functional groups to transport resveratrol. Nonetheless, a higher adsorption capacity

usually leads to a reduced drug release since the drug-MSM interaction is so strong that the release of the drug can be compromised. Naghiloo *et al*. synthesized and modified SBA-16 with amino groups to carry ibuprofen [17], and once again, the functionalization of this silica improved the drug loading capacity compared to the non-functionalized system. Nonetheless, in this case, the functionalization also increased the ibuprofen release. According to the authors, this behavior could be due to the less ordered structure, surface density, and polarity of functional groups.

In this study, cephalexin (CFX, Scheme 1) has been chosen as a model drug. CFX is an antibiotic used to treat respiratory and genitourinary tract infections, otitis media, and skin structure infections, among others [18]. It is a zwitterionic molecule, which means that it can have different behaviors according to the pH of the dissolution medium. CFX has a short half-life (ca. 1.1 h), so it is prescribed 3-4 times a day to maintain effective doses in the bloodstream [19]. Therefore, it could be interesting to control the CFX release for a prolonged period to reduce the posology and increase patient compliance. In this sense, CFX has been previously loaded into functionalized and non-functionalized SBA-15 [20,21]. Nonetheless, to the best of our knowledge, no similar previous studies have reported about KIT-6 and modified KIT-6 as CFX carriers. Furthermore, KIT-6 porous materials present a different morphology concerning SBA-15, called cage-like with interconnected cubic mesostructure in 3D [22]. Thus, this structural difference could represent interesting results between both systems.

The purpose of this work is to study the loading and *in vitro* release of CFX using synthetic KIT-6 and amino-groups functionalized KIT-6 (KIT-6/NH_2) as supports (see Scheme 1). The influence of functionalization and textural properties on the CFX loading and release were addressed at different temperature and pH conditions. Furthermore, the

in vitro biocompatibility and the CFX *in vitro* release kinetic from KIT-6 and KIT-6/NH_2 materials were also explored.

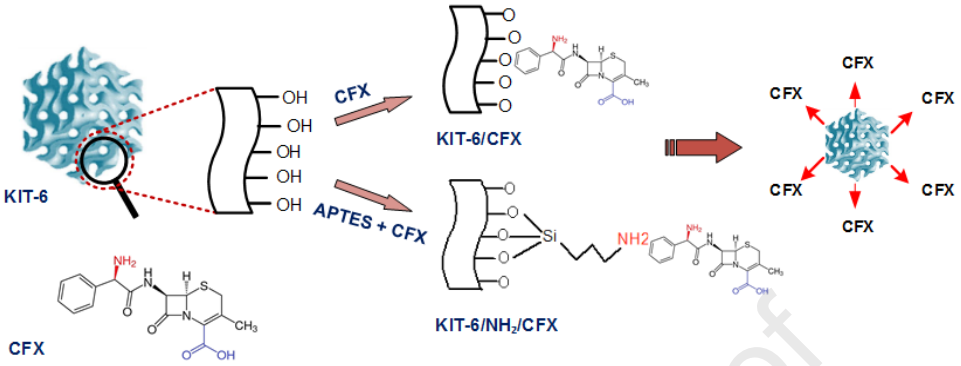

Scheme 1 Schematic representation of loading and controlled release of CFX using KIT-6 and KIT-6/NH_2 carriers.

2. Materials and methods

2.1 Synthesis and functionalization of mesoporous silica KIT-6

The mesoporous silica (KIT-6) used in this study was synthesized by a sol-gel method based on previous works [23]. The reagents used in the synthesis were: Pluronic P123 (EO_{20}-PO_{70}-EO_{20}) (Sigma Aldrich) used as pore structure-directing agent; tetraethyl orthosilicate (TEOS, Si $C_8H_{20}O_4$, Merck) as silica source; HCl (Merck) as catalyst and *n*-butanol (Merck) and H_2O as solvents. The final molar ratio of each reagent was (0.017 P123: 1 TEOS: 1.83 HCl: 1.31 C_4H_9OH: 195 H_2O). Pluronic P123 was firstly dissolved in an HCl solution under vigorous stirring (35 °C). Then, *n*-butanol was added, and the stirring was kept for 1 h. Afterward, TEOS was added directly to the solution, and the resulting mixture was stirred for 24 h at 35 °C. Subsequently, the mixture was aged for 24 h at 95 °C under static conditions. The precipitate formed during the aging was washed

with deionized water until the conductivity was 10 μS cm^{-1}. The obtained solid was dried at 60 °C for 12 h and calcined (350 °C, 6 h) with a heating rate of 1 °C min^{-1}.

The amine-functionalization of mesoporous silica KIT-6 was performed via post-synthesis grafting [24], employing 3-aminopropyl-triethoxysilane (APTES, Sigma Aldrich) as a functionalizing agent. The amount of APTES was determined assuming a stoichiometric reaction (1:1) between KIT-6 surface silanol groups (-SiOH) and methoxy groups (-OMe) of the organosilane molecule [25]. Therefore, from the surface concentration of silanol groups for KIT-6 calcined at 350 °C (2.8 Si OH/nm^2) [26,27] and the surface area of this material (1040 m^2 g^{-1}), was found the amount of APTES (4.82 mmol) that can saturate all silanol groups in a gram of KIT-6. The procedure consisted of dispersing 1 g of KIT-6 in 60 mL of dry toluene (Biopack). Then, the corresponding amount of APTES (4.82 mmol) was added to the mixture and kept under reflux and N_2 atmosphere for 24 h at 80 °C. Finally, the resulting solid was filtered, washed with toluene, and dried at 40 °C in vacuum for 12 h. The resultant sample is referred to as KIT-6/NH_2.

2.2 Cephalexin stability at different temperatures

The temperature stability of CFX in solution was evaluated to optimize the drug loading process conditions on KIT-6. As an acceptance criterion for stability, an upper and lower limit of 10 % of the original concentration of CFX was established. The procedure of this test is detailed in the S1 (ESI).

2.3 Cephalexin drug loading

149 To study CFX loading, different amounts (0.01, 0.02, 0.03, 0.05 and 0.07 g) of KIT-6 or
150 KIT-6/NH_2 were dispersed in 20 mL of CFX solution (1 mg mL^{-1}, pH:6). The mixture
151 was left in contact for 8 h at 30 °C under constant agitation. Samples were withdrawn
152 and filtered through 0.45 µm Millipore® (S) membranes. The CFX concentration
153 remaining in the solution was quantified by UV-Vis spectrophotometer (262 nm) as an
154 indirect method. The CFX amount (q_t) was calculated with equation (1),

155

$$q_t = \frac{(C_o - C_t) \cdot V}{W} \quad \text{(Eq. 1)}$$

156 where q_t is the total amount of CFX per gram of KIT-6 (mg g^{-1}) at a specific time; C_o is
157 the initial concentration of CFX before being in contact with adsorbent material (mg mL^{-1});
158 C_t is the final aqueous phase concentration after removing the adsorbent material (mg
159 mL^{-1}); V is the volume of CFX solution used in the experiment (mL), and W is the mass
160 of KIT-6 (mg). The samples obtained after drug adsorption were named KIT-6/CFX and
161 KIT-6/NH_2/CFX.

162

163 *2.4 Characterization of MSM samples*

164 X-ray powder diffraction (XRD) analysis was performed using a diffractometer (X'Pert
165 Pro model, Malven Panalytical) equipped with a solid-state detector (X'Celerator) and a
166 spinning sample holder. The diffractogram patterns were recorded using random oriented
167 mounts with CuKα radiation (λ=0.154 nm), with a step of 0.02° operating at 45 kV and
168 40 mA.

169 Fourier-transform infrared spectroscopy (FTIR) spectra of the samples KIT-6, KIT-
170 6/NH_2, KIT-6/CFX, and KIT-6/NH_2/CFX were obtained with a JASCO 6200 apparatus

171 equipped with a Ge ATR. Analyses were performed from 400 to 4000 cm^{-1} with a
172 resolution of 2 cm^{-1} (100 scans/sample).
173 Nitrogen adsorption-desorption isotherms were measured at 77 K using manometric
174 adsorption equipment (ASAP 2000, Micromeritics). The samples were previously
175 outgassed at 60 °C for 12 h. The specific surface area (S_{BET}) was obtained by Brunauer,
176 Emmet and Teller method [28]. The total pore volume (V_{TP}) was calculated using
177 Gurvich's rule at a relative pressure of 0.98 [29]. Micropore volume ($V_{\mu P}$) and primary
178 mesopores volumes (V_{PMP}) were obtained by the α_S-plot method [30]. Secondary
179 mesopores volume (V_{SMP}) was calculated by the difference ($V_{TP} - (V_{\mu P} + V_{PMP})$). The
180 pore size distributions (PSD) were obtained with ASiQWin software, Quantachrome
181 Instruments, using the NLDFT method (N_2 on silica at 77K cylindrical pores, NLDFT
182 equilibrium model).
183 High-Resolution Transmission Electron Microscopy (HR-TEM) studies were
184 performed in FEI Titan G2 60-300 microscope coupled with analytical electron
185 microscopy (AEM) performed with a SUPER-X silicon-drift windowless energy-
186 dispersive X-ray spectroscopy detector (EDX). The samples were deposited onto
187 copper grids (300 mesh coated by farmvar/carbon film, Agar Scientific). The
188 morphology of the samples was also evaluated through scanning electron
189 microscopy (SEM). SEM microphotographs were obtained using an FEI Quanta 200
190 microscope. The samples were coated with a gold film (10 nm).
191 X-ray photoelectron spectra (XPS) were performed on a Physical Electronics PHI 5701
192 spectrometer. A non-monochromatic Mg-Kα radiation (720 μm, 300 W, 15 kV, 1253.6
193 eV) and a multi-channel detector were employed. Samples were analyzed in a constant
194 pass energy mode at 29.35 eV. Charge referencing was measured against C 1*s* od

195 adventitious carbon at 284.8 eV. The PHI ACCESS ESCA-V6.0 F software package and
196 Multipak v8.2b were used for acquisition and data analysis, respectively. Recorded
197 spectra were fitted using Gauss-Lorentz curves in order to determine the binding energy
198 of the different element core levels more accurately.
199 Thermogravimetric analysis (TGA) (TGA-50H, Shimadzu) was performed using a
200 vertical oven and a precision of 1.0 $x10^{-6}$ g. Approximately 0.04 g of each sample were
201 weighed in aluminum sample pans. The tests were performed from 30 to 1000 °C (10
202 $^{o}C \cdot min^{-1}$) in an air atmosphere.
203

204 *2.5 Cephalexin stability at different pH*

205 One of the aims of this work was to test the formulations of the KIT-6 and KIT-6/NH_2
206 mesopore materials (previously loaded with CFX) in oral controlled release tests.
207 However, prior to the *in vitro* release tests, the CFX stability was evaluated in two media:
208 (i) simulated gastric fluid (pH: 1.2) and (ii) simulated intestinal fluid (pH: 6.8) without
209 enzymes [31]. These tests were performed for CFX, KIT-6/CFX, and KIT-6/NH_2/CFX.
210 Further information can be found in S2 (ESI).
211

212 *2.6 In vitro CFX release tests*

213 KIT-6/CFX and KIT-6/NH_2/CFX composites, with a dose of 0.015 g of CFX, were
214 suspended in 50 mL of either 0.001 M HCl (pH:1.2, gastric environment) or phosphate
215 buffer (pH: 6.8, intestinal environment). Dialysis membranes of 12-14000 Da cutoff were
216 used to retain the composite (KIT-6 or KIT-6/NH_2) without interfering with CFX (347.39
217 Da). The whole system was kept at a constant temperature of 37 ºC (thermostatic bath)

and agitated at ~100 rpm. Samples aliquots (1 mL) were collected at predetermined time intervals and subsequently replenished the same volume of physiological solutions to maintain sink conditions. The samples were filtered (0.45 µm Millipore® (S)) and CFX quantified by UV-Vis spectroscopy (257 y 262 nm for acid and neutral pH, respectively). In order to evaluate the mechanism that controls the kinetic process of drug release, different mathematical models can be used, e.g., zero-order, first-order, second-order, Hixon-Crowell, Weibull, Korsmeyer-Peppas, among others [32]. For the particular case of drug release systems from ordered mesoporous materials, there is no exact model to adjust the release profiles, but the profiles could be adjusted to any of the models described above. In this study, the model that best fit was the Korsmeyer-Peppas [33]. This model is described by equation 2, where M_t is equal to the drug released and M_o is the total amount of drug-loaded, k is the release rate constant, and n es the diffusional exponent that informs the release mechanism. Values of $n \leq 0.5$ report a Fickian or quasi Fickian diffusion, and n = 0.5-1 indicates an anomalous mechanism for the drug release. The criteria that were taken into account for the selection of the Peppas model as that one with the best fit were: (i) the correlation coefficient (R^2 close to 1) and (ii) the Akaike Information Criterion (AIC) that is a measure of the quality of fit based on maximum probability when comparing multiple models for a data series [34]. In particular, the lowest the AIC value, the better the model fitting. The AIC is given by equation 3, where n is the number of dissolution data, p is the number of parameters in the model, and $WSSR$ is the sum of the squares of the residuals.

$$M_t/M_0 = kt^n \quad \text{(Eq. 2)}$$

$$AIC = n\ln(WSSR) + 2p \quad \text{(Eq. 3)}$$

2.7 In vitro biocompatibility studies

The biocompatibility of samples KIT-6/CFX and KIT-6/NH_2/CFX was tested through MTT tests (3-(4,5-dimethylthiazol-2-yl)-2,5-diphenyltetrazolium bromide) by using Caco-2 human colorectal adenocarcinoma cell lines which were obtained from the American Type Culture Collection (ATCC, USA). The cells were grown in Dulbecco's modified Eagle medium (DMEM, Sigma Aldrich®-Merck, Milan, Italy), supplemented with 10 % fetal bovine serum (FBS, Euroclone, Milan, Italy), 200 IU mL^{-1} penicillin, and 0.2 mg mL^{-1} streptomycin (PBI International, I), kept at 37 ºC in a 5 % CO_2 atmosphere with 95 % relative humidity. Caco-2 cells were seeded in 96-well plates (35000 cells/well) and subsequently grown until sub-confluence. Afterward, well-plates were washed with saline solution, and the cell substrates were put in contact with KIT-6/CFX and KIT-6/NH_2/CFX samples at different concentrations (100, 500, and 1000 µg mL^{-1}). After 24 hours of sample/Caco-2 cells contact, the biocompatibility was tested by adding 2.5 mg mL^{-1} of MTT into the culture medium. This test is based on the activity of mitochondrial dehydrogenases, which convert MTT in formazan crystals in living cells. After 3 hours, 100 µL of dimethyl sulfoxide solution were added to each well (DMSO, Sigma-Aldrich®-Merck, Milan, Italy) to dissolve formazan salts. The absorbance was assayed at 570 nm/655 nm using an ELISA plate reader (Imark Absorbance Reader, Bio-rad, Hercules, CA, USA).

3. Results and discussion

3.1 Cephalexin stability at different temperatures

The temperature effect on CFX stability in an aqueous solution is shown in Fig. 1. CFX concentration decreases with increasing temperature and time at pH 6. For CFX

refrigerated solutions (2 - 8 °C), the concentration remained stable over time. On the other hand, solutions exposed at room temperature (25 °C) showed a gradual CFX decomposition of 8 % and 12 % after 8 and 24 hours, respectively. An 18 % less concentration was found after 72 h in solution. Solutions subjected to 30 °C were less stable, losing up to 22 % after 72 h. The increase in temperature could have produced a hydrolytic reaction causing instability in the CFX molecules [35]. Despite the results, aqueous dissolutions of CFX (pH 6) can be considered stable until 8 h at both 25 and 30 ºC since the amount of decomposed CFX within this period was considered non-significant for the scope of the study. Based on these results, the CFX loading onto KIT-6 and KIT-6/NH_2 platforms was carried out at 30 °C for a maximum of 8 h.

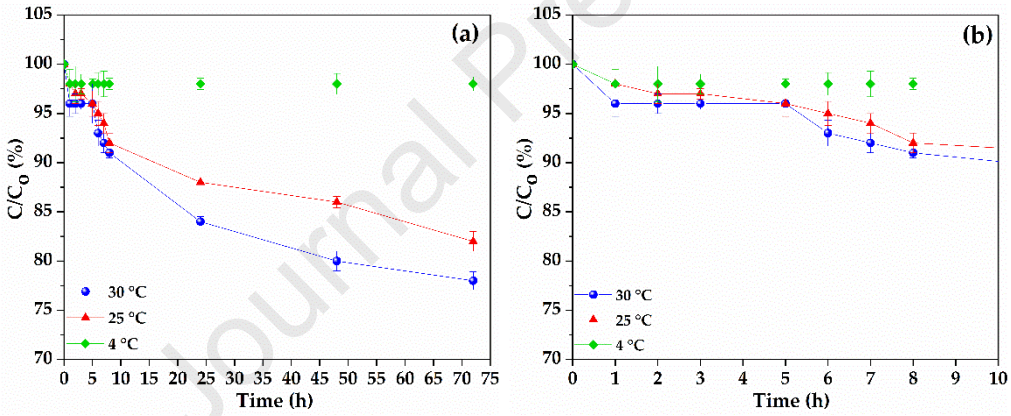

Fig. 1 CFX stability profiles at different temperatures (a) from 0 to 72 h and (b) enlarging of (a) from 0 to 10 h (mean values ± s.d.; n = 3).

3.2 Cephalexin drug loading

The effect of the mass amount of KIT-6 and KIT-6/NH_2 adsorbents on CFX loading capacity are included in Fig. 2. These results reveal that there was no significant difference in the total amount adsorbed by both samples. Different authors affirm that properties such as large specific surface area and high total pore volume of the supports

282 enable the encapsulation of drugs with a large loading capacity [36–38]. However, in this
283 study, although the textural properties of KIT-6/NH_2 were significantly reduced by
284 functionalization (as detailed below in point 3.3, table 1), the total amount of CFX
285 adsorbed was similar for both KIT-6 and KIT/NH_2. Therefore, the CFX adsorption
286 capacity of KIT-6/NH_2 could probably be related to the attractive electrostatic
287 interactions that occur between the protonated amino groups on the functionalized silica
288 surface and the deprotonated carboxyl groups on the CFX molecule. In Fig. 2 is also
289 possible to observe that drug loading capacity increases when the adsorbent (KIT-6 and
290 KIT-6/NH_2) mass decrease. This result could be attributed to an aggregation of the silica
291 particles, which caused a reduction in the interfacial area between the CFX solution and
292 the adsorbent. Similar behaviors have been found in other previously published studies
293 [39,40]. Based on these results, the lowest dose (10 mg) was chosen that allowed loading
294 the largest amount of drug, 200 mg g^{-1} for KIT-6 and 195 mg g^{-1} for KIT-6/NH_2. These
295 samples were characterized by the different techniques shown below and finally were
296 used in the release tests.

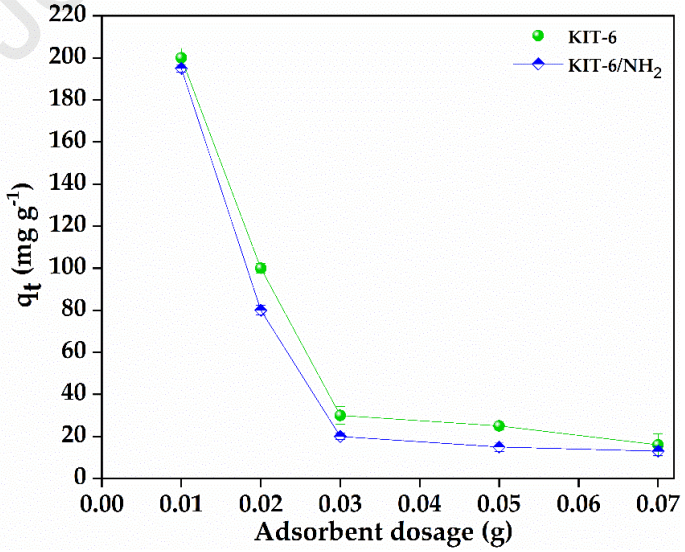

297

298 **Fig. 2** Adsorbent amount effect on CFX adsorption (mean values ± s.d.; n = 3).

3.3 Characterization of MSM samples

The small-angle XRD patterns of the KIT-6 and KIT-6/NH_2 samples before and after drug loading are presented in Fig. 3. It is observed that the KIT-6 material exhibits a very intense diffraction peak at 2θ~ 0.8 attributed to the (211) plane and two less intense peaks at 2θ~1.4 and 2θ~1.6 corresponding to the (321) and (420), respectively. These peaks confirm the bicontinuous cubic *Ia3d* symmetry reported for KIT-6, with a high degree of structural order [41]. The same diffraction peaks are also observed in the KIT-6/NH_2 sample, which shows that the amount of grafted functional groups did not modify the structural order of the starting material. However, these samples loaded with CFX show a significant decrease in the intensity of the diffraction peaks, which likely is due to the introduction of the drug inside the pores, causing a decrease in the scattering contrast between the pores and side walls of silica [42].

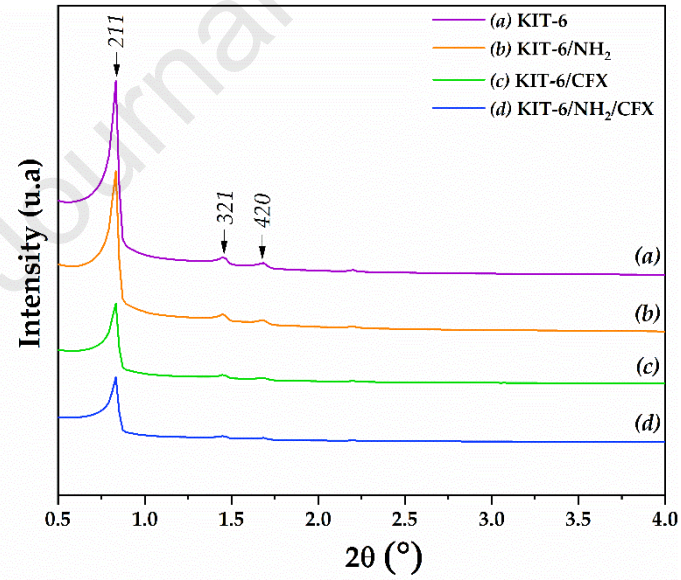

Fig. 3 Small-angle XRD patterns of (a) KIT-6, (b) KIT-6/NH_2, (c) KIT-6/CFX and (d) KIT-6/NH_2/CFX.

Fig. 4 shows FTIR spectra of loaded and unloaded nanocomposites. Typical vibrations of KIT-6 were present. The broad band at 3000 - 3700 cm^{-1} was associated with –OH

316 groups ascribed to the physisorbed water on the silica surface. The bands at 1080 and
317 800 cm^{-1} correspond to the asymmetric and symmetric stretchings from Si-O-Si bonds,
318 while the band at 960 cm^{-1} is due to the stretching of silanol groups (Si-OH). The Si-O-
319 Si stretching causes a vibration band at 460 cm^{-1} [43]. The amino functionalization of
320 KIT-6 (KIT-6/NH_2) was confirmed due to the appearance of additional characteristic
321 FTIR bands (Fig. 4b). Less intensity is observed in the region of 3000-3700 cm^{-1}, where
322 the characteristic band of the NH_2 groups (3460 cm^{-1}) overlaps with that of the -OH
323 groups [44], evidencing the presence of NH_2 KIT-6 surface. In addition, the bands at
324 1560 and 2937 cm^{-1} correspond to the N-H stretching and C-H bending vibration of the
325 primary amine.
326 CFX adsorption on the two nanocomposites was confirmed by FTIR spectra. The pure
327 CFX spectrum (Fig. 4c) shows characteristic bands between 3400-3200 cm^{-1} associated
328 with the stretching vibrations of the amino groups, and at 3040 and 2945 cm^{-1} are due to
329 the acidic hydroxyl groups and the C-H stretching vibrations, respectively. Likewise, the
330 bands that appear at 1759 and 1689 cm^{-1} are due to the four-membered lactam carbonyl
331 and secondary amine carbonyl groups, respectively. Other adsorption bands observed at
332 1589, 1396 and 1290 cm^{-1} correspond to the stretching vibrations of the N-H, C-H and
333 C-N bonds, while the bands at 1072 and 694 cm^{-1} are due to the bonds C-O and C-S [45].
334 After the incorporation of CFX, changes in the original spectra of both materials are
335 noted. For KIT-6/CFX (Fig. 4d), new bands appear at 1388, 1590, 1656 and 1758 cm^{-1}
336 corresponding to the C-H, N-H and C=O bonds identified in the spectrum of the pure
337 drug. Moreover, in the KIT-6/NH_2/CFX sample (Fig. 4e), these same bands appear,
338 confirming the presence of the drug in both samples, however in the bands of the
339 functionalized nanocomposite some differences are observed with respect to the pure

nanocomposite. The first difference is the highest intensity in the bands at 1388 and 1590 cm^{-1}, due to the contribution of the C-H and N-H bonds by APTES and the drug. The second difference is observed in the reduction in the intensity of the bands at 1656 and 1758 cm^{-1}. This behavior probably is due to an electrostatic interaction produced between the CFX carbonyl groups and the protonated amino groups; this same behavior has been observed in previous studies on functionalized mesoporous silica [46].

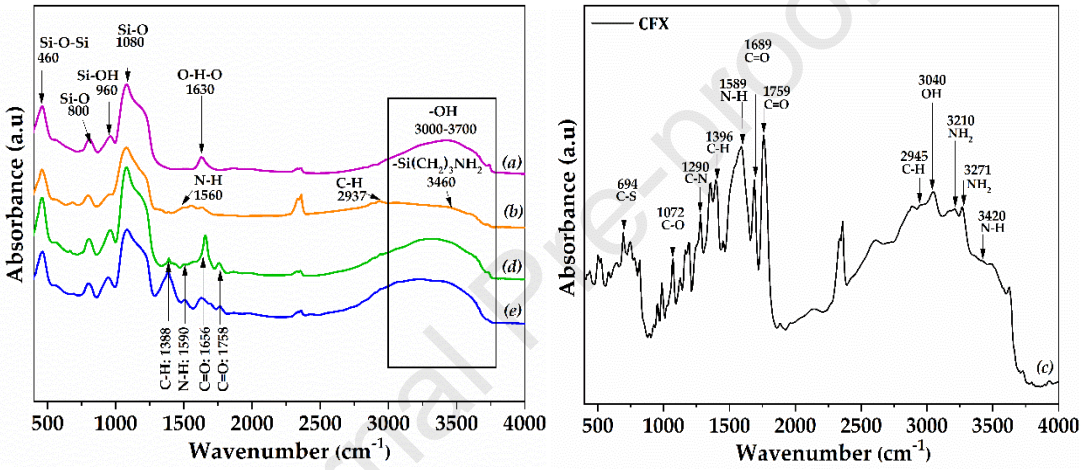

Fig. 4 FTIR spectra of (a) KIT-6, (b) KIT-6/NH_2, (c) CFX, (d) KIT-6/CFX and (e) KIT-6/NH_2/CFX.

Fig. 5 presents N_2 adsorption-desorption isotherms at 77 K of KIT-6 and KIT-6/NH_2 samples before and after CFX loading. According to the IUPAC classification, the four samples present type IV (a) isotherms [47]. The KIT-6, KIT-6/NH_2, and KIT-6/NH_2/CFX exhibit a type H1 hysteresis loop, indicating the presence of highly ordered mesopores. In these samples, the adsorption-desorption branches in the hysteresis loop are parallel, a characteristic of materials with uniform pore size and a narrow distribution in pore size. Moreover, the KIT-6/CFX exhibits an unusual H5 hysteresis loop associated with particular structures containing open and partially blocked mesopores, probably due to

the presence of CFX. It can also be noted that KIT-6 isotherm presents a pronounced capillary condensation stage at high relative pressures (0.6 p/p^o), suggesting the presence of large mesopores, which are slightly reduced due to the incorporation of functional groups. In KIT-6/CFX, the capillary condensation is not so pronounced and begins at a lower relative pressure (0.45 p/p^o) compared to KIT-6. Consequently, it is possible to infer that mesopores have been occupied by CFX molecules. Besides, the adsorption-desorption branches are not parallel, indicating that the pore size distribution is not uniform. Lastly, KIT-6/NH_2/CFX shows capillary condensation steps at higher pressures than KIT-6/NH_2.

The textural properties were obtained from the nitrogen isotherms data, (Table 1). It is observed that KIT-6 has a high specific surface area, with a significant presence of mesopores and a small amount of micropores. However, once the KIT-6 has been modified with amino groups and loaded with CFX molecules, these textural properties values considerably decrease, particularly the micropores, which were likely covered by the functional groups and CFX molecules. The change in the texture of the materials under study indicates that the incorporation of functional groups and the loaded CFX molecules have been achieved in both the surface and the mesopores of the silica materials.

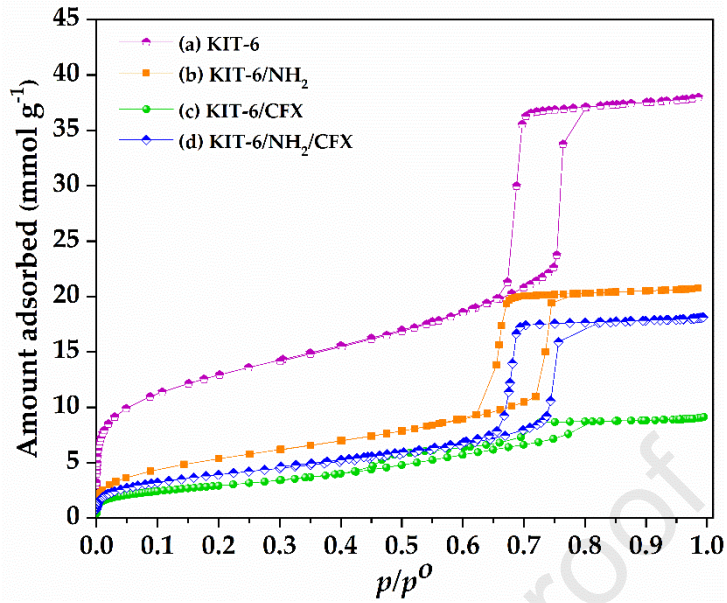

Fig. 5 N_2 adsorption-desorption isotherms at 77 K of (a) KIT-6, (b) KIT-6/NH_2, (c) KIT-6/CFX and (d) KIT-6/NH_2/CFX.

Table 1 Textural properties of the mesoporous silica materials

Samples	S_{BET} ($m^2\ g^{-1}$)	V_{TP} ($cm^3\ g^{-1}$)	$V_{\mu P}$ ($cm^3\ g^{-1}$)	V_{PMP} ($cm^3\ g^{-1}$)	V_{SMP} ($cm^3\ g^{-1}$)
KIT-6	1040	1.32	0.07	1.14	0.11
KIT-6/NH_2	440	0.72	0	0.69	0.03
KIT-6/CFX	240	0.32	0	0.29	0.03
KIT-6/NH_2/CFX	320	0.63	0	0.60	0.03

The pore size distribution of the silica samples are shown in Fig. 6. It is observed that pure KIT-6 is a highly ordered mesoporous silica with mesopore sizes around 8.5 nm. Likewise, this material presents a small contribution in the region of micropores with a pore size around 1.0 nm. KIT-6 mesoporous size was reduced to 7.8 nm after the incorporation of amino groups. The micropores can not be seen after this treatment, probably because they were covered with APTES molecules. On the other hand, when KIT-6 is in contact with the CFX, the porosity changes significantly. One noticeable change is the appearance of two new contributions in the PSD, around 5 nm and 9.2 nm,

390 which indicates that CFX occupies and blocks a large part of the mesopores. In contrast,
391 KIT-6/NH_2 showed an increase in mesopore size after CFX loading, probably due to the
392 CFX interact with NH_2 occupying the primary mesopores region [48].

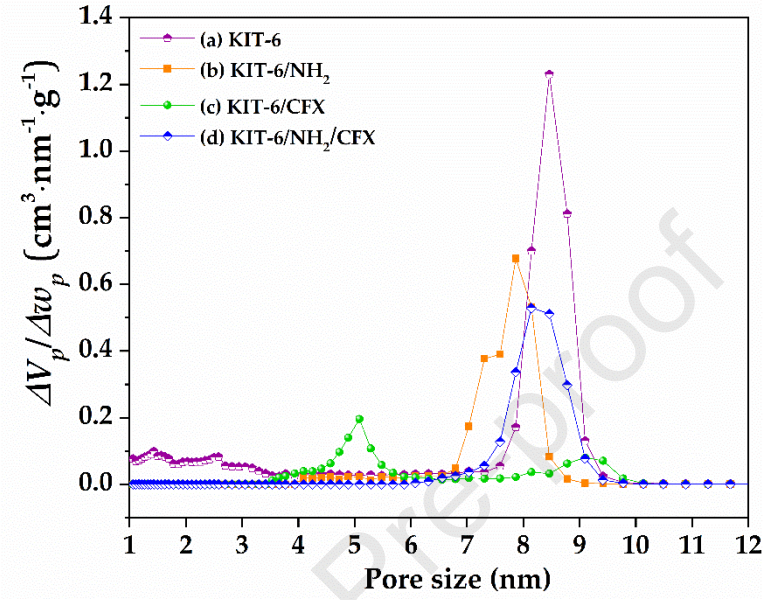

393

394 **Fig. 6** Pore size distribution of (a) KIT-6, (b) KIT-6/NH_2, (c) KIT-6/CFX and (d) KIT-
395 6/NH_2/CFX.

396 HR-TEM microphotographs and EDX mapping of KIT-6, KIT-6/NH_2, KIT-6/CFX, and
397 KIT-6/NH_2/CFX are gathered in Fig. 7. In Fig. 7a, it can be seen that KIT-6 shows its
398 typical highly ordered mesoporous structure with interconnected cubic mesopores in 3D,
399 results that agree with others reported elsewhere [23,49,50]. In the KIT-6/NH_2 sample
400 (Fig. 7b), a high ordering of interconnected porosity in 3D is also evidenced. However,
401 there is a slight decrease in the mesoporous channels, indicating that part of the amine
402 functional groups was anchored within the mesopores (see yellow magnification).
403 On the other hand, KIT-6/CFX (Fig. 7c) and KIT-6/NH_2/CFX (Fig. 7d) also conserved
404 their highly ordered porous structure. However, due to the incorporation of the drug the
405 mesoporous channels were contracted (Fig. 7a to 7d; this is mainly observed in KIT-

406 6/CFX because this sample loaded more drug inside its pores, which agrees with obtained
407 results from the nitrogen adsorption-desorption isotherms and the PSD. Additionally,
408 through EDX and maps, it was possible to evidence the components of both samples;
409 KIT-6/CFX (Fig. 7e, f) contains silica (Si, O) and CFX (C, O, N, S). KIT-6/NH_2/CFX
410 (Fig. 7g, h) contains silica (Si, O), functional amino groups (C, O, Si, N), and CFX (C,
411 O, N, S). It can be noted that KIT-6/NH_2/CFX detected a peak of N more intense that
412 KIT-6/CFX since this sample contains N from the amino groups and CFX. In addition,
413 through the maps, it was possible to corroborate a homogeneous distribution of each of
414 the constituents in the porous structure of both materials.

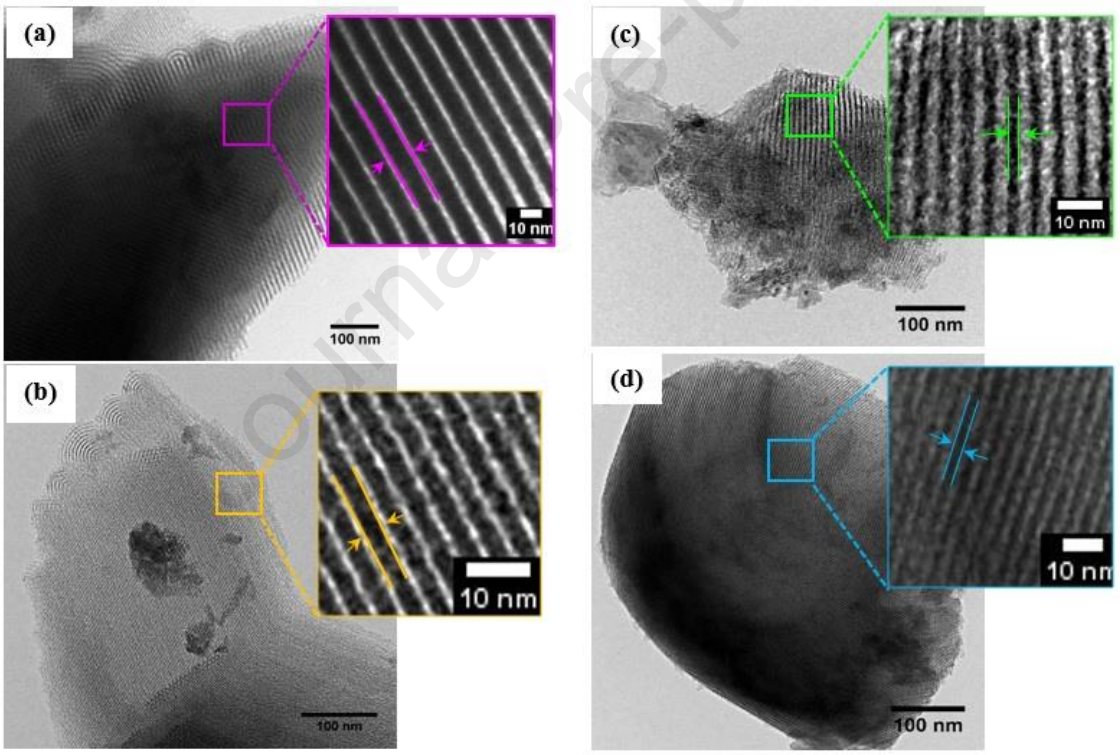

415

416

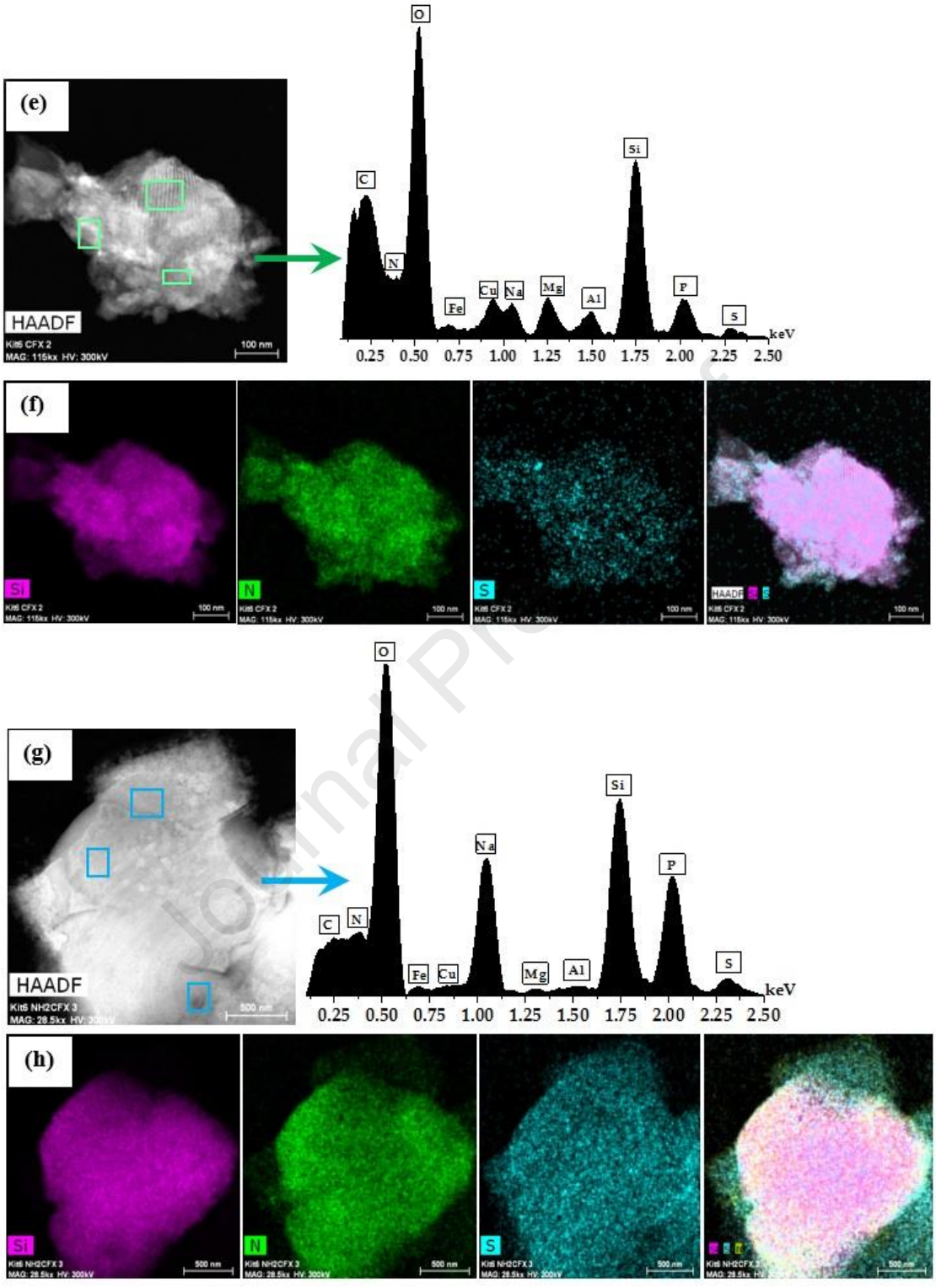

417

418

419 **Fig. 7** HR-TEM micrographs of (a) KIT-6, (b) KIT-6/NH_2, (c) KIT-6/CFX, (d) KIT-

420 6/NH_2/CFX, (e, f) EDX and mapping of KIT-6/CFX, and (g, h) EDX and mapping of

421 KIT-6/NH_2/CFX.

SEM studies (Fig. 8) showed differences such as CFX crystallization in KIT-6 and KIT-6/NH_2 before and after drug loading. KIT-6 (Fig. 8a) and KIT-6/NH_2 (Fig. 8b) did not present significant differences indicating that the functionalization did not affect the morphology of the silica. During the loading of drugs onto inorganic platforms, drug precipitation and crystallization may occur. This precipitation phenomenon could influence the drug release profile, showing a burst release effect due to the rapid dissolution of drug crystals over the inorganic platform [51]. In this case, no morphological differences have been found between KIT-6, KIT6/NH_2, KIT-6/CFX, and KIT-6/NH_2/CFX, thus proving the absence of drug crystals.

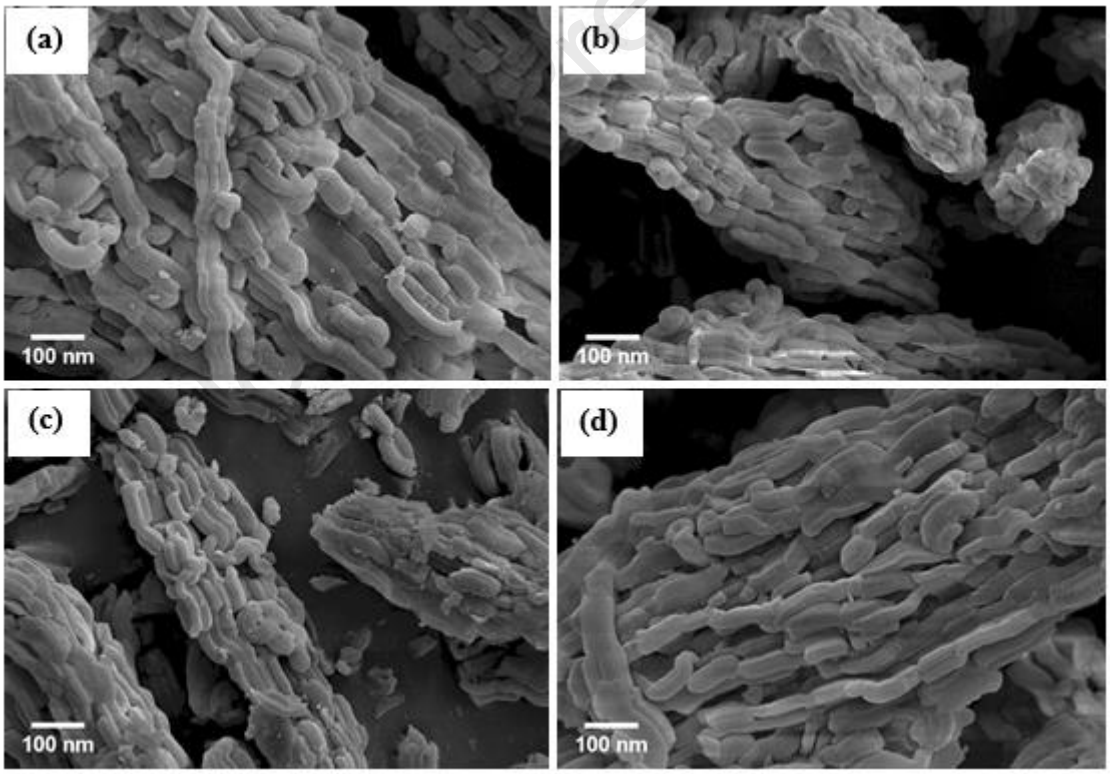

Fig. 8 SEM micrographs of (a) KIT-6, (b) KIT-6/NH_2, (c) KIT-6/CFX and (d) KIT-6/NH_2/CFX.

435 XPS analysis was carried out to study the surface chemistry of KIT-6, KIT-6/NH_2, KIT-
436 6/CFX, KIT-6/NH_2/CFX, the deconvolution of the most representative peaks (C and N)
437 are shown in Fig. 9. KIT-6 presents the C 1*s* peak with two energy bands at 284.8 and
438 286.5 eV corresponding to the C-H and C-O bonds, respectively. The same bands are
439 observed in KIT-6/NH_2 and KIT-6/NH_2/CFX but with greater intensity in both cases.
440 This higher intensity is due to the presence of C-Si and C-N bonds established by APTES
441 and CFX.
442 Likewise, the core level N 1*s* spectrum of KIT-6/NH_2 presents two contributions at 399.0
443 and 401.4 eV, indicating the presence of two types of nitrogen on the surface of the
444 samples. The first and most abundant at 399.0 eV is assigned to free amino groups (-
445 NH_2), and the second, at 401.4 eV to protonated amino groups (-NH_3^+) [52]. Moreover,
446 the incorporation of CFX in KIT-6 and KIT-6/NH_2 causes some changes in the N 1*s*
447 core-level spectra bands at 399.5, 401.5 and 403.0 eV, and they are assigned to -NH_2, -
448 NH_3^+ and N-H, respectively. In KIT-6/CFX, these bands are less intense since the -NH_2
449 group present belongs only to the CFX, while in the functionalized sample, the intensity
450 of these bands is higher due to the presence of amino groups from both the APTES and
451 CFX. An increase in the intensity of the band at 401 eV can be observed, likely due to
452 the acid pH of the CFX solution in the adsorption process protonated the free amino
453 groups.
454 Table 2 shows the atomic concentration of the elements found on the surface of all
455 samples under study. Functionalization of KIT-6/NH_2 was successful, as indicated by the
456 2.8 % of N 1*s* detected. Likewise, the amount of N 1*s* in the KIT-6/CFX sample was
457 lower (0.6) than in KIT-6/NH_2/CFX (2.3). This result indicates that beyond the fact that

in the KIT-6/CFX sample, there were only N 1*s* contributions from CFX, the major part of CFX molecules enter the inner porosity of KIT-6, also in agreement with PSD results.

Table 2 Atomic concentration of elements detected in KIT-6, KIT-6/NH_2, KIT-6/CFX and KIT-6/NH_2/CFX

Element	Atomic concentration (%)			
	KIT-6	KIT-6/NH_2	KIT-6/CFX	KIT-6/NH_2/CFX
C 1*s*	4.6	18.3	10.3	15.5
N 1*s*	-	2.8	0.6	2.3
O 1*s*	68.2	54.5	62.7	58.0
Na 1*s*	-	-	2.2	1.3
Si 2*p*	27.1	24.3	24.1	22.8

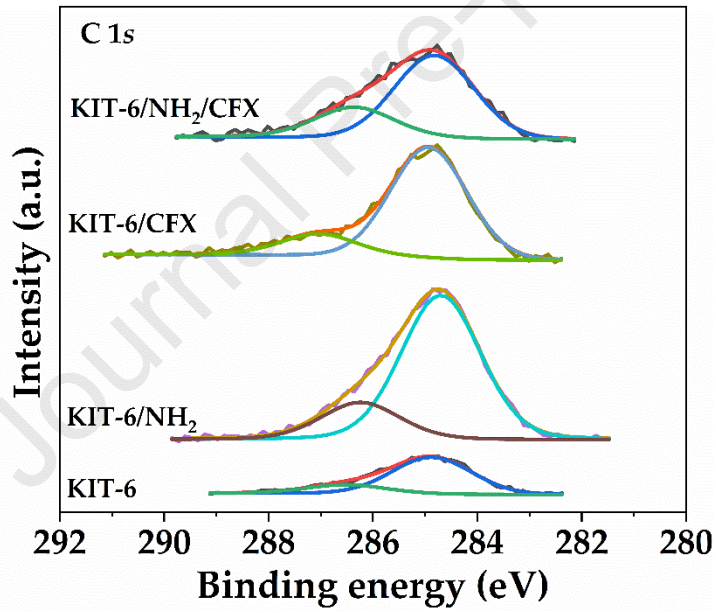

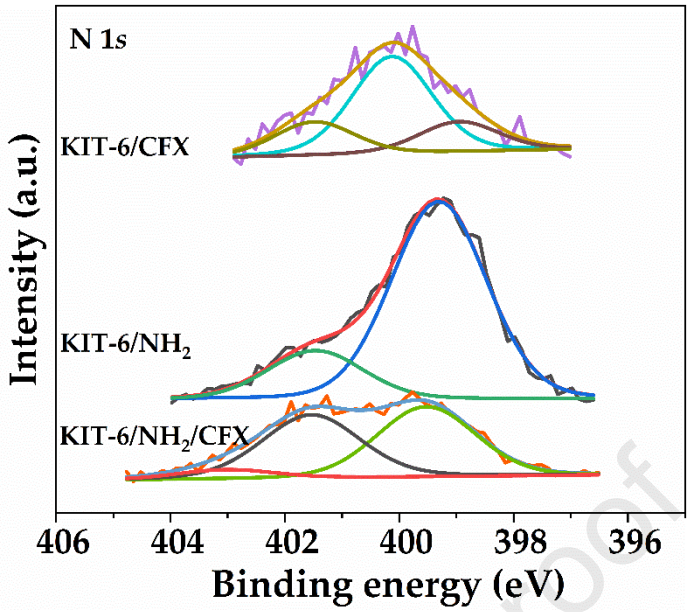

Fig. 9 Deconvolution of C 1*s* and N 1*s* spectra.

TGA analyses (Fig. 10) were carried out to study the degree of functionalization and to confirm the drug loading capacity of all systems. All samples showed a first event around 50 ºC that can be ascribed to the loss of physisorbed water [20]. From 300 °C, a progressive weight loss of about 9 % is observed in KIT-6, possibly due to the condensation of silanol groups [53]. In the functionalized counterpart (KIT-6/NH_2), a weight-loss event of 6.8 % is observed from 150 °C up to 640 °C, which corresponds to the thermal decomposition of the aminopropyl chains that were anchored on the surface of the KIT-6. This result is important evidence of the degree of functionalization, which was also confirmed by the XPS experimental data where an atomic nitrogen concentration of 2.8 % was found. CFX-loaded samples (KIT-6/CFX and KIT-6/NH_2/CFX) showed a much more pronounced weight loss event from 200 ºC with respect to the sample merely functionalized (KIT-6/NH_2), demonstrating the presence of the drug in both materials. This result is agrees with other reports where the pure CFX shows an exothermic event at 203 ºC [54]. Finally, it can be seen that there is no

significant difference in total weight loss in both samples; 14.6 and 12.5% were obtained for KIT-6/CFX and KIT-6/NH_2/CFX, respectively. This result agrees with the adsorption tests in solution where a slightly higher load capacity was found for the pure material.

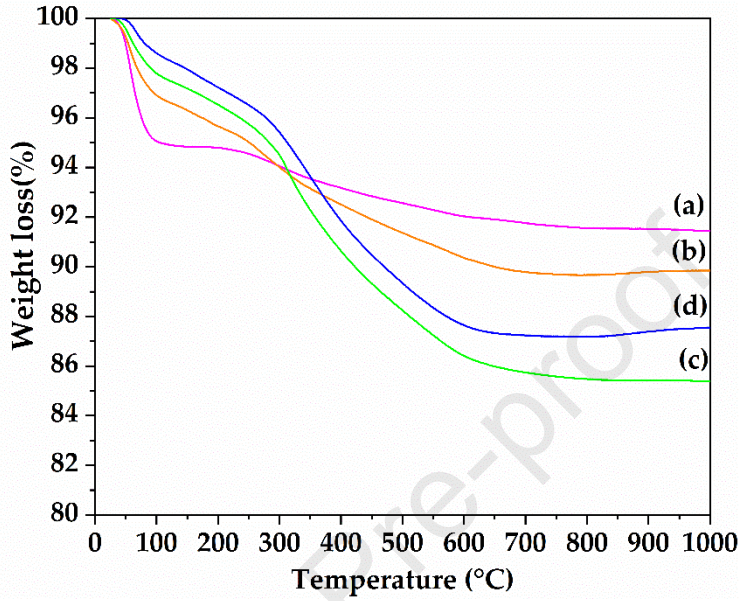

Fig. 10 TGA curves of (a) KIT-6, (b) KIT-6/NH_2, (c) KIT-6/CFX and (d) KIT-6/NH_2/CFX.

3.4 Cephalexin stability at different pH

An additional stability study was carried out on the loaded composites (KIT-6/CFX and KIT-6/NH_2/CFX), and it was compared with the pure drug. Fig. 11 shows the change in CFX initial concentration as a function of pH and time. Major changes in CFX concentration can be observed at pH 6.8, with a 36 % of CFX loss after 24 hours. This finding indicates that the active principle of CFX is more stable in gastric conditions than in the intestinal ones, likely because the intestinal pH coincides with the dissociation equilibrium (pKa_2 6.8) of the α-amino group of the CFX molecule [55,56]. However, when CFX is adsorbed on KIT-6 (Fig. 11a) and KIT-6/NH_2 (Fig. 11b), occurs an

498 important change in the stability. This change is more noticeable at pH 6.8 than at pH
499 1.2, since the decrease in concentration at 24 h goes from 36 % to 10 % in the case of
500 KIT-6/CFX and 36 % to 2 % in the case of KIT-6/NH_2/CFX. These results are promising
501 since they indicate that porous silica protects the CFX from the potential degradation
502 caused by gastric and intestinal pHs.

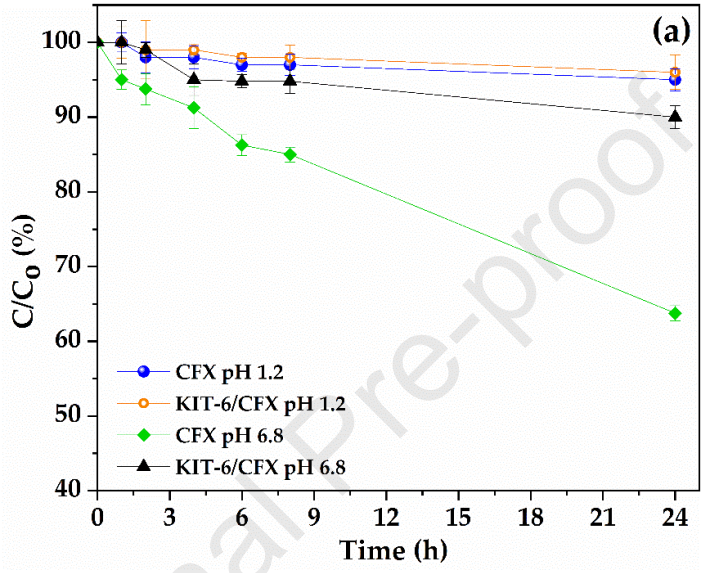

503

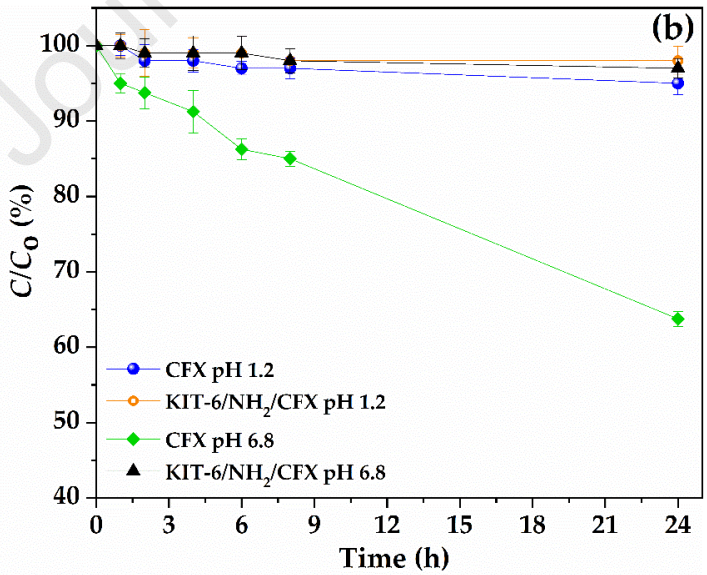

504

505 **Fig. 11** Stability profiles at gastric pH (1.2) and intestinal pH (6.8) of (a) CFX and KIT-
506 6 (b) CFX and KIT-6/NH_2 at 37 °C (mean values ± s.d.; n = 3).

3.5 In vitro CFX release tests

In vitro release profiles of CFX are shown in Fig. 12. It can be seen that pure CFX is completely dissolved in a short time, both in gastric and intestinal media (total drug dissolution in 30 min and 1 h, respectively). In an acid pH, CFX is mainly constituted (~99 %) by [$CFXH^+$] cation due to the protonation of the amino group [NH_3^+]. On the other hand, in a more basic environment, CFX is conformed by 50 % of the zwitterionic species [$CFX^{\pm}$], that is, the amino group is protonated –NH_3^+ and the carboxylic acid group is deprotonated –COO^-. In addition, the other 50 % is conformed by the anionic species [CFX^-] generated by the loss of the proton associated with the amino group [57]. A slower CFX release can be observed when the drug is loaded in KIT-6 and KIT-6/NH_2, reaching a plateau after 12 h. As it can be seen, the total percentage of drug released was higher for KIT-6/CFX than KIT-6/NH_2/CFX. This difference is probably due to the nature of drug-platform interactions between KIT-6 and CFX, mainly formed by weak van der Waals forces, where the lone pair of electrons of the carboxylic oxygen of CFX forms a partial bond with the silanol groups of KIT-6 [58]. On the other hand, attractive electrostatic interactions can be established between the protonated amino group of KIT-6/NH_2 and the –COO^- group of CFX, making CFX molecules remain "trapped" in the nanocomposite.

Another relevant factor in the release process is the pH. The acid environment produced a CFX dissolution rate that reached the release equilibrium in ~3h. Likely, CFX has specific alkaline properties that accelerate its dissolution [4]. Likewise, the total amount of CFX released in acid conditions (pH 1.2) is lower than in an alkaline environment (pH 6.8), although the sample is functionalized or not. We hypothesize that this is due to H^+ in the gastric fluid, reinforcing the interactions between the protonated amino groups

present in the walls of the KIT-6 and KIT-6/NH_2 mesoporous matrices, respectively. In a basic environment, the repulsive electrostatic interactions predominate between the deprotonated carboxylic group of CFX and the deprotonated silanol group of KIT-6. Moreover, the CFX loaded in KIT-6/NH_2 was easily protonated and, therefore, weakened the drug-silica interactions, leading to a much more drug release.

Table 3 shows the parameters calculated from Korsmeyers-Peppas model for the experimental data of the release profiles of the pure CFX and KIT-6/CFX and KIT-6/NH_2/CFX samples at gastric and intestinal pH. In all samples, a satisfactory linear correlation was observed with R^2 values close to 1 and negative AIC values that denote a good fit to the model employed. On the other hand, it is also observed $n < 0.5$ in all cases, which indicates that a release mechanism occurs by Fickian diffusion [59]. According to this kinetic, CFX would be dissolving in the interior of the mesoporous channels, and subsequently, they must diffuse through the composite toward the dissolution medium. Thus, CFX release is governed by the nature of the chemical interactions established between the drug and the mesoporous silica and by a diffusion process through the porous structure of the composites. The porous arrangement and morphology of KIT-6 (interconnected cubic 3D-mesopores with a cage-like morphology) can also have some influence on the release profiles. The CFX has been previously loaded in other silica materials as the well-known SBA-15, which has a mesopore structure with a 2-D hexagonal arrangement and rod-like morphology [21]. Comparing those reported results with these obtained with KIT-6, the release kinetics of the latter is slower and the maximum amount released is reached in a longer time (24 h) than in the SBA-15 material (10 h), which has a less complex porous structure.

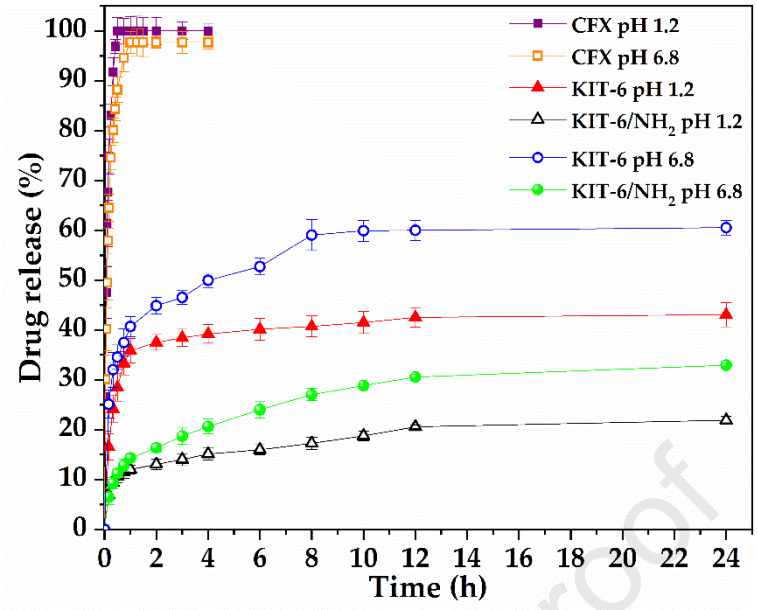

554

555 **Fig. 12** *In vitro* release profiles of CFX using mesoporous silica KIT-6 and KIT-6/NH_2

556 at pH 1 and 6.8 (mean values ± s.d.; n = 5).

557 **Table 3** Kinetic release parameters for CFX release from KIT-6 and KIT-6/NH_2
558 materials
559

Sample	Release medium	Korsmeyer-Peppas			
		k (h-1)	n	R^2	AIC
CFX	pH 1.2	1.031	0.221	0.740	-24.573
	pH 6.8	1.030	0.221	0.885	-25.316
KIT-6	pH 1.2	0.313	0.130	0.750	-29.210
	pH 6.8	0.392	0.165	0.953	-59.844
KIT-6/NH_2	pH 1.2	0.115	0.206	0.978	-94.640
	pH 6.8	0.136	0.297	0.980	-78.751

560
561
562 *3.6 In vitro biocompatibility tests*
563
564 The biocompatibility of KIT-6/CFX and KIT-6/NH_2/CFX was examined using MTT test
565 [60], and the results are shown in Fig. 13. Both samples demonstrated total
566 biocompatibility against Caco-2 cells, indicating that any of the samples exerted harmful
567 effects over cells at any of the concentrations tested. In fact, the cell survival rate

remained above 90 %, even at the highest concentration (1000 µg mL^{-1}). To our knowledge, this is one of the few cell viability studies performed on KIT-6/CFX and KIT-6/NH_2/CFX materials with such a high concentration of MTT. According to previous studies, it has been found that specific properties of MSM can influence biocompatibility. For example, silica particles with a higher surface area have been shown to produce more oxidative stress, leading to lower cell viability [61], Therefore, the surface area of the KIT-6 and KIT-6/NH_2 have not caused changes in cell viability. In fact, it has been demonstrated that amino functionalization has positive effects on cell viability due to the improvement of electrostatic interactions between amino groups and negative charges on the Caco-2 cell surface that can influence the attachment of the particles to cells and subsequent cell signaling [62].

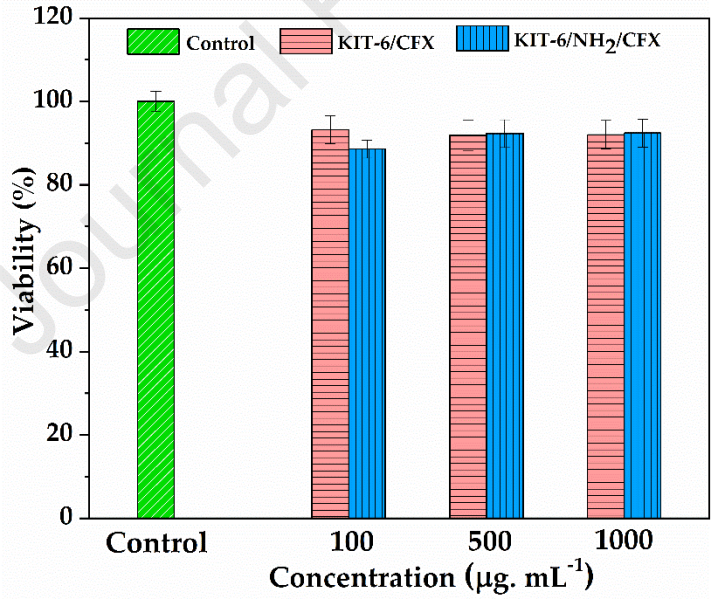

Fig. 13 MTT tests of CFX loaded samples. Cellular viability (%) vs. KIT-6/CFX and KIT-6/NH_2/CFX concentration. Caco-2 cells were used, and the sample contact was kept for 24 h (mean values ± s.d.; n = 7).

4. Conclusions

Ordered mesoporous silica KIT-6 was synthesized and modified with functional amino groups (KIT-6/NH_2). Both materials were tested as carriers in the loading and controlled release of CFX. It was found that the loading capacity is governed by the textural properties such as high specific surface area, high total pore volume for KIT-6, and mainly by the chemical interactions between amino groups anchored on silica and the carboxyl of CFX for KIT-6/NH_2. On the other hand, KIT-6 and KIT-6/NH_2 showed a good performance in the controlled release of CFX at gastric and intestinal pH, where silica with functional groups prevent early release. However due to its strong interaction with the drug, it presented lower release percentage than non-functionalized silica. The release profiles were adjusted to the Korsmeyer-Peppas model, which indicates that CFX release is mainly governed by diffusion, probably produced from the highly ordered mesopores of the cubic structure to the dissolution medium. Furthermore, it was found that both samples are biocompatible against Caco-2 cells. These results confirm that KIT-6 and KIT-6/NH_2 materials are promising carriers for CFX adsorption and controlled release systems.

Acknowledgements

The authors thank Laboratorios Puntanos of Argentina for donating the drug (cephalexin) used in this study.

Funding sources

This work was supported by the Consejo Nacional de Investigaciones Científicas y Técnicas (CONICET); the Unversidad Nacional de San Luis, Argentina (UNSL); the

608 SEGIB-Carolina Foundation and the Universidad Nacional Autónoma de Nicaragua-
609 Managua.

610

611 **References**

612

613 [1] V. Fathi Vavsari, G. Mohammadi Ziarani, A. Badiei, The role of SBA-15 in drug
614 delivery, RSC Adv. 5 (2015) 91686–91707. https://doi.org/10.1039/c5ra17780d.
615 [2] K. Montiel-Centeno, D. Barrera, J. Villarroel-Rocha, J.J. Arroyo-Gómez, M.S.
616 Moreno, K. Sapag, CMK-3 nanostructured carbon: Effect of temperature and time
617 carbonization on textural properties and H_2 storage, Chem. Eng. Commun. 206
618 (2019) 1581–1595. https://doi.org/10.1080/00986445.2019.1615469.
619 [3] M. Manzano, M. Vallet-Regí, Mesoporous Silica Nanoparticles for Drug
620 Delivery, Adv. Funct. Mater. 30 (2020) 1902634.
621 https://doi.org/10.1002/adfm.201902634.
622 [4] Q.Z. Zhai, X.D. Li, Immobilization and sustained release of cefalexin on MCF
623 nano-mesoporous material, J. Dispers. Sci. Technol. 40 (2019) 1675–1685.
624 https://doi.org/10.1080/01932691.2019.1615936.
625 [5] C.F. Toncón-Leal, S. Amaya-Roncancio, A.A. García Blanco, M.S. Moreno, K.
626 Sapag, Confined Iron Nanoparticles on Mesoporous Ordered Silica for Fischer–
627 Tropsch Synthesis, Top. Catal. 62 (2019) 1086–1095.
628 https://doi.org/10.1007/s11244-019-01201-1.
629 [6] K. Montiel-Centeno, D. Barrera, J. Villarroel-Rocha, M.S. Moreno, K. Sapag,
630 Hierarchical nanostructured carbons as CO2 adsorbents, Adsorption. 25 (2019)
631 1287–1297. https://doi.org/10.1007/s10450-019-00089-3.
632 [7] L. Chen, M. Liu, Q. Zhou, X. Li, Recent developments of mesoporous silica
633 nanoparticles in biomedicine, Emergent Mater. 3 (2020) 381–405.
634 https://doi.org/10.1007/s42247-020-00078-1.
635 [8] A.C. de J. Oliveira, L.L. Chaves, F. de O.S. Ribeiro, L.R.M. de Lima, T.C.
636 Oliveira, F. García-Villén, C. Viseras, R.C.M. de Paula, P.J. Rolim-Neto, F.
637 Hallwass, E.C. Silva-Filho, D. Alves da Silva, J.L. Soares-Sobrinho, M.F. de L.R.

638 Soares, Microwave-initiated rapid synthesis of phthalated cashew gum for drug
639 delivery systems, Carbohydr. Polym. 254 (2020) 117226.
640 https://doi.org/10.1016/j.carbpol.2020.117226.
641 [9] A. Borrego-Sánchez, R. Sánchez-Espejo, F. García-Villén, C. Viseras, C. Ignacio
642 Sainz-Díaz, Praziquantel–clays as accelerated release systems to enhance the low
643 solubility of the drug, Pharmaceutics. 12 (2020) 1–16.
644 https://doi.org/10.3390/pharmaceutics12100914.
645 [10] M. Martínez-Carmona, M. Colilla, M.L. Ruiz-González, J.M. González-Calbet,
646 M. Vallet-Regí, High resolution transmission electron microscopy: A key tool to
647 understand drug release from mesoporous matrices, Microporous Mesoporous
648 Mater. 225 (2016) 399–410. https://doi.org/10.1016/j.micromeso.2016.01.019.
649 [11] K.B. Seljak, P. Kocbek, M. Gašperlin, Mesoporous silica nanoparticles as delivery
650 carriers: An overview of drug loading techniques, J. Drug Deliv. Sci. Technol. 59
651 (2020). https://doi.org/10.1016/j.jddst.2020.101906.
652 [12] S. Kim, M.J. Stébé, J.L. Blin, A. Pasc, PH-controlled delivery of curcumin from
653 a compartmentalized solid lipid nanoparticle@mesostructured silica matrix, J.
654 Mater. Chem. B. 2 (2014) 7910–7917. https://doi.org/10.1039/c4tb01133c.
655 [13] A. Aguilar-Colomer, M. Colilla, I. Izquierdo-Barba, C. Jiménez-Jiménez, I.
656 Mahillo, J. Esteban, M. Vallet-Regí, Impact of the antibiotic-cargo from MSNs on
657 gram-positive and gram-negative bacterial biofilms, Microporous Mesoporous
658 Mater. 311 (2021) 110681. https://doi.org/10.1016/j.micromeso.2020.110681.
659 [14] J. Ortiz-Bustos, A. Martín, V. Morales, R. Sanz, R.A. García-Muñoz, Surface-
660 functionalization of mesoporous SBA-15 silica materials for controlled release of
661 methylprednisolone sodium hemisuccinate: Influence of functionality type and
662 strategies of incorporation, Microporous Mesoporous Mater. 240 (2017) 236–245.
663 https://doi.org/10.1016/j.micromeso.2016.11.021.
664 [15] M.M. Ayad, N.A. Salahuddin, A.A. El-Nasr, N.L. Torad, Amine-functionalized
665 mesoporous silica KIT-6 as a controlled release drug delivery carrier,
666 Microporous Mesoporous Mater. 229 (2016) 166–177.
667 https://doi.org/10.1016/j.micromeso.2016.04.029.
668 [16] L. Latifi, S. Sohrabnezhad, Influence of pore size and surface area of mesoporous
669 silica materilas (MCM-41 and KIT-6) on the drug loading and release, J. Sol-Gel

Sci. Technol. 87 (2018) 626–638. https://doi.org/10.1007/s10971-018-4742-7.

[17] M. Naghiloo, M. Yousefpour, M.S. Nourbakhsh, Z. Taherian, Functionalization of SBA-16 silica particles for ibuprofen delivery, J. Sol-Gel Sci. Technol. 74 (2015) 537–543. https://doi.org/10.1007/s10971-015-3631-6.

[18] A.A. Salarian, Y. Bahari Mollamahale, Z. Hami, M. Soltani-Rezaee-Rad, Cephalexin nanoparticles: Synthesis, cytotoxicity and their synergistic antibacterial study in combination with silver nanoparticles, Mater. Chem. Phys. 198 (2017) 125–130. https://doi.org/10.1016/j.matchemphys.2017.05.059.

[19] D. Kundu, T. Banerjee, Development of microcrystalline cellulose based hydrogels for the in vitro delivery of Cephalexin, Heliyon. 6 (2020) e03027. https://doi.org/10.1016/j.heliyon.2019.e03027.

[20] M. Legnoverde, I. Jiménez-Morales, A. Jimenez-Morales, E. Rodriguez-Castellon, E. Basaldella, Modified Silica Matrices for Controlled Release of Cephalexin, Med. Chem. (Los. Angeles). 9 (2013) 672–680. https://doi.org/10.2174/15734064113090500006.

[21] M.S. Legnoverde, E.I. Basaldella, Influence of particle size on the adsorption and release of cephalexin encapsulated in mesoporous silica SBA-15, Mater. Lett. 181 (2016) 331–334. https://doi.org/10.1016/j.matlet.2016.06.053.

[22] R. Guillet-Nicolas, R. Ahmad, K.A. Cychosz, F. Kleitz, M. Thommes, Insights into the pore structure of KIT-6 and SBA-15 ordered mesoporous silica-recent advances by combining physical adsorption with mercury porosimetry, New J. Chem. 40 (2016) 4351–4360. https://doi.org/10.1039/c5nj03466c.

[23] T.B. Benzaquén, D.A. Barrera, P.M. Carraro, K. Sapag, O.M. Alfano, G.A. Eimer, Nanostructured catalysts applied to degrade atrazine in aqueous phase by heterogeneous photo-Fenton process, Environ. Sci. Pollut. Res. 26 (2019) 4192–4201. https://doi.org/10.1007/s11356-018-2348-9.

[24] A. Vinu, K.Z. Hossain, K. Ariga, Recent advances in functionalization of mesoporous silica, J. Nanosci. Nanotechnol. 5 (2005) 347–371. https://doi.org/10.1166/JNN.2005.089.

[25] A. Olea, E.S. Sanz-Pérez, A. Arencibia, R. Sanz, G. Calleja, Amino-functionalized pore-expanded SBA-15 for CO 2 adsorption, Adsorption. 19 (2013) 589–600. https://doi.org/10.1007/s10450-013-9482-y.

[26] V.Y. Davydov, A. V. Kiselev, L.T. Zhuravlev, Study of the surface and bulk hydroxyl groups of silica by infra-red spectra and D2O-exchange, Trans. Faraday Soc. 60 (1964) 2254–2264. https://doi.org/10.1039/TF9646002254.

[27] L.T. Zhuravlev, Concentration of Hydroxyl Groups on the Surface of Amorphous Silicas, Langmuir. 3 (1987) 316–318. https://pubs.acs.org/sharingguidelines (accessed January 25, 2022).

[28] S. Brunauer, P.H. Emmett, E. Teller, Adsorption of Gases in Multimolecular Layers, J. Am. Chem. Soc. 60 (1938) 309–319. https://doi.org/10.1021/ja01269a023.

[29] F. Rouquerol, J. Rouquerol, K. Sing, Adsorption by powders and porous solids, Wiley, San Diego, 1999. https://doi.org/10.1002/vipr.19990110317.

[30] J. Villarroel-Rocha, D. Barrera, A. Blanco, M. Jalil, K. Sapag, Importance of the αs-plot method in the characterization of nanoporous materials, Adsorpt. Sci. Technol. 31 (2013) 165–183. https://doi.org/10.1260/0263-6174.31.2-3.165.

[31] A. Borrego-Sánchez, E. Carazo, C. Aguzzi, C. Viseras, C.I. Sainz-Díaz, Biopharmaceutical improvement of praziquantel by interaction with montmorillonite and sepiolite, Appl. Clay Sci. 160 (2018) 173–179. https://doi.org/10.1016/j.clay.2017.12.024.

[32] J. Siepmann, F. Siepmann, Mathematical modeling of drug dissolution, Int. J. Pharm. 453 (2013) 12–24. https://doi.org/10.1016/j.ijpharm.2013.04.044.

[33] R.W. Korsmeyer, R. Gurny, E. Doelker, P. Buri, N.A. Peppas, Mechanisms of solute release from porous hydrophilic polymers, Int. J. Pharm. 15 (1983) 25–35. https://doi.org/10.1016/0378-5173(83)90064-9.

[34] J.E. Cavanaugh, A.A. Neath, The Akaike information criterion: Background, derivation, properties, application, interpretation, and refinements, Wiley Interdiscip. Rev. Comput. Stat. 11 (2019) e1460. https://doi.org/10.1002/wics.1460.

[35] S.M. Mitchell, J.L. Ullman, A.L. Teel, R.J. Watts, PH and temperature effects on the hydrolysis of three β-lactam antibiotics: Ampicillin, cefalotin and cefoxitin, Sci. Total Environ. 466–467 (2014) 547–555. https://doi.org/10.1016/j.scitotenv.2013.06.027.

[36] M. Vallet-Regí, M. Manzano, J.M. González-Calbet, E. Okunishi, Evidence of

drug confinement into silica mesoporous matrices by STEM spherical aberration corrected microscopy, Chem. Commun. 46 (2010) 2956–2958. https://doi.org/10.1039/C000806K.

[37] M. Martínez-Carmona, Y.K. Gun'ko, M. Vallet-Regí, Mesoporous Silica Materials as Drug Delivery: "The Nightmare" of Bacterial Infection, Pharm. 2018, Vol. 10, Page 279. 10 (2018) 279. https://doi.org/10.3390/PHARMACEUTICS10040279.

[38] Y. He, L. Luo, S. Liang, M. Long, H. Xu, Amino-functionalized mesoporous silica nanoparticles as efficient carriers for anticancer drug delivery, J. Biomater. Appl. 32 (2017) 524–532. https://doi.org/10.1177/0885328217724638.

[39] A. Mehrizad, K. Zare, H. Aghaie, S. Dastmalchi, Removal of 4-chloro-2-nitrophenol occurring in drug and pesticide waste by adsorption onto nano-titanium dioxide, Int. J. Environ. Sci. Technol. 9 (2012) 355–360. https://doi.org/10.1007/S13762-012-0038-6/TABLES/1.

[40] F.Y. Wang, H. Wang, J.W. Ma, Adsorption of cadmium (II) ions from aqueous solution by a new low-cost adsorbent-Bamboo charcoal, J. Hazard. Mater. 177 (2010) 300–306. https://doi.org/10.1016/j.jhazmat.2009.12.032.

[41] Y. Doi, A. Takai, Y. Sakamoto, O. Terasaki, Y. Yamauchi, K. Kuroda, Tailored synthesis of mesoporous platinum replicas using double gyroid mesoporous silica (KIT-6) with different pore diameters via vapor infiltration of a reducing agent, Chem. Commun. 46 (2010) 6365–6367. https://doi.org/10.1039/C0CC01196G.

[42] S. Jangra, P. Girotra, V. Chhokar, V.K. Tomer, A.K. Sharma, S. Duhan, In-vitro drug release kinetics studies of mesoporous SBA-15-azathioprine composite, J. Porous Mater. 3 (2016) 679–688. https://doi.org/10.1007/S10934-016-0123-1.

[43] C. Pirez, J.C. Morin, J.C. Manayil, A.F. Lee, K. Wilson, Sol-gel synthesis of SBA-15: Impact of HCl on surface chemistry, Microporous Mesoporous Mater. 271 (2018) 196–202. https://doi.org/10.1016/j.micromeso.2018.05.043.

[44] J. Goscianska, A. Olejnik, I. Nowak, APTES-functionalized mesoporous silica as a vehicle for antipyrine – adsorption and release studies, Colloids Surfaces A Physicochem. Eng. Asp. 533 (2017) 187–196. https://doi.org/10.1016/j.colsurfa.2017.07.043.

[45] A. Hajikarimi, M. Sadeghi, Free radical synthesis of cross-linking gelatin base

poly NVP/acrylic acid hydrogel and nanoclay hydrogel as cephalexin drug deliver, J. Polym. Res. 27 (2020) 57. https://doi.org/10.1007/s10965-020-2020-1.

[46] V. Nairi, L. Medda, M. Monduzzi, A. Salis, Adsorption and release of ampicillin antibiotic from ordered mesoporous silica, J. Colloid Interface Sci. 497 (2017) 217–225. https://doi.org/10.1016/J.JCIS.2017.03.021.

[47] M. Thommes, K. Kaneko, A. V. Neimark, J.P. Olivier, F. Rodriguez-Reinoso, J. Rouquerol, K.S.W. Sing, Physisorption of gases, with special reference to the evaluation of surface area and pore size distribution (IUPAC Technical Report), Pure Appl. Chem. 87 (2015) 1051–1069. https://doi.org/10.1515/pac-2014-1117.

[48] J. Goscianska, A. Olejnik, I. Nowak, M. Marciniak, R. Pietrzak, Ordered mesoporous silica modified with lanthanum for ibuprofen loading and release behaviour, Eur. J. Pharm. Biopharm. 94 (2015) 550–558. https://doi.org/10.1016/j.ejpb.2015.07.003.

[49] J. Fan, J. Zhang, P. Solsona, S. Suriñach, M.D. Baró, J. Sort, E. Pellicer, Nanocasting synthesis of mesoporous SnO_2 with a tunable ferromagnetic response through Ni loading, RSC Adv. 6 (2016) 104799–104807. https://doi.org/10.1039/c6ra23918h.

[50] J. Wang, Y. Li, Z. Zhang, Z. Hao, Mesoporous KIT-6 silica-polydimethylsiloxane (PDMS) mixed matrix membranes for gas separation, J. Mater. Chem. A. 3 (2015) 8650–8658. https://doi.org/10.1039/c4ta07127a.

[51] Z. Ulker, C. Erkey, An emerging platform for drug delivery: Aerogel based systems, J. Control. Release. 177 (2014) 51–63. https://doi.org/10.1016/j.jconrel.2013.12.033.

[52] S. Ravi, S. Zhang, Y.R. Lee, K.K. Kang, J.M. Kim, J.W. Ahn, W.S. Ahn, EDTA-functionalized KCC-1 and KIT-6 mesoporous silicas for Nd^{3+} ion recovery from aqueous solutions, J. Ind. Eng. Chem. 67 (2018) 210–218. https://doi.org/10.1016/j.jiec.2018.06.031.

[53] A. El-Fiqi, M. Bakry, Facile and rapid ultrasound-mediated synthesis of spherical mesoporous silica submicron particles with high surface area and worm-like mesoporosity, Mater. Lett. 281 (2020) 128620. https://doi.org/10.1016/j.matlet.2020.128620.

[54] L.P. Manelli, Cephalexin, Anal. Profiles Drug Subst. Excipients. 4 (1975) 21–46.

https://doi.org/10.1016/S0099-5428(08)60007-6.

[55] M.S. Legnoverde, S. Simonetti, E.I. Basaldella, Influence of pH on cephalexin adsorption onto SBA-15 mesoporous silica: Theoretical and experimental study, Appl. Surf. Sci. 300 (2014) 37–42. https://doi.org/10.1016/j.apsusc.2014.01.198.

[56] P.M. Quizon, B. Abrahamsson, R. Cristofoletti, D.W. Groot, A. Parr, P. Langguth, J.E. Polli, V.P. Shah, T. Tajiri, M.U. Mehta, J. Dressman, Biowaiver Monographs for Immediate Release Solid Oral Dosage Forms : Cephalexin Monohydrate, 109 (2020) 1846–1862. https://doi.org/10.1016/j.xphs.2020.03.025.

[57] T. Hatanaka, S. Morigaki, T. Aiba, K. Katayama, T. Koizumi, Effect of pH on the skin permeability of a zwitterionic drug, cephalexin, Int. J. Pharm. 125 (1995) 195–203. https://doi.org/10.1016/0378-5173(95)00113-W.

[58] B. V. Bhaskara Rao, R. Mukherji, G. Shitre, F. Alam, A.A. Prabhune, S.N. Kale, Controlled release of antimicrobial Cephalexin drug from silica microparticles, Mater. Sci. Eng. C. 34 (2014) 9–14. https://doi.org/10.1016/j.msec.2013.10.002.

[59] E.B. Lim, T.A. Vy, S.W. Lee, Comparative release kinetics of small drugs (ibuprofen and acetaminophen) from multifunctional mesoporous silica nanoparticles, J. Mater. Chem. B. 8 (2020) 2096–2106. https://doi.org/10.1039/c9tb02494h.

[60] E. Grela, J. Kozłowska, A. Grabowiecka, Current methodology of MTT assay in bacteria – A review, Acta Histochem. 120 (2018) 303–311. https://doi.org/10.1016/J.ACTHIS.2018.03.007.

[61] K. Letchmanan, S.C. Shen, W.K. Ng, R.B.H. Tan, Enhanced dissolution and stability of artemisinin by nano-confinement in ordered mesoporous SBA-15 particles, J. Microencapsul. 32 (2015) 390–400. https://doi.org/10.3109/02652048.2015.1035684.

[62] A. Zakeri Siavashani, M. Haghbin Nazarpak, F. Fayyazbakhsh, T. Toliyat, S.J.P. McInnes, M. Solati-Hashjin, Effect of amino-functionalization on insulin delivery and cell viability for two types of silica mesoporous structures, J. Mater. Sci. 51 (2016) 10897–10909. https://doi.org/10.1007/s10853-016-0301-1.

Cephalexin loading and controlled release studies on mesoporous silica functionalized with amino groups

Kiara Montiel-Centeno[a,b], Deicy Barrera[a], Fátima García-Villén[b], Rita Sánchez-Espejo[b], Ana Borrego-Sánchez[b], Enrique Rodríguez-Castellón[c], Giuseppina Sandri[d] César Viseras[b,e*], Karim Sapag[a*]

[a.] *Laboratorio de Sólidos Porosos. Instituto de Física Aplicada. CONICET. Universidad Nacional de San Luis. Ejército de los Andes 950. CP: 5700 – San Luis. Argentina.*

[b.] *Deparment of Pharmacy and Pharmaceutical Technology, University of Granada, 18071 Granada, Spain.*

[c.] *Departamento de Química Inorgánica, Unidad Asociada al Instituto de Catálisis (CSIC), Facultad de Ciencias, Universidad de Málaga, 29071 Málaga, España.*

[d.] *Deparment of Drug Sciences, University of Pavia, viale Tatamelli 12, 22100 Pavia, Italy.*

[e.] *Andalusian Institute of Earth Sciences (Consejo Superior de Investigaciones Científicas-University of Granada) Armilla, 18100 Granada, Spain.*

Highlights

- Amino-functionalized KIT-6 mesoporous silica in controlled release of cephalexin.
- Amino groups influence the drug-carrier interaction.
- KIT-6 pure and functionalized protect cephalexin from intestinal degradation.
- Amino-functionalized KIT-6 mesoporous silica are biocompatible in Caco-2 cells.

Graphical Abstract

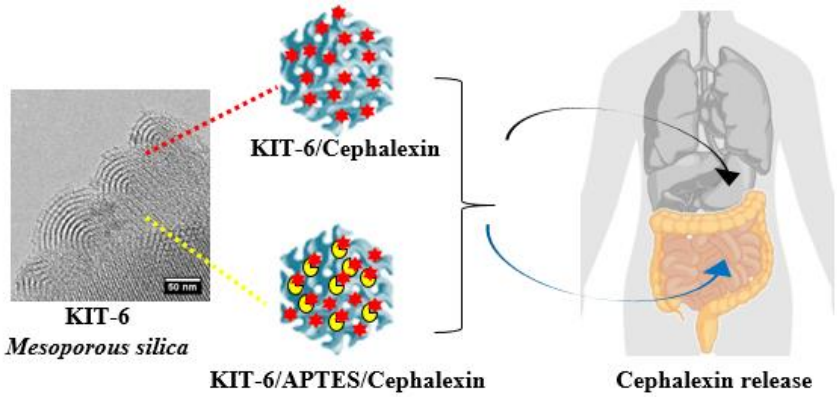

Cephalexin loading and controlled release studies on mesoporous silica functionalized with amino groups

Kiara Montiel-Centeno[a,b], Deicy Barrera[a], Fátima García-Villén[b], Rita Sánchez-Espejo[b], Ana Borrego-Sánchez[b], Enrique Rodríguez-Castellón[c], Giuseppina Sandri[d] César Viseras[b,e*], Karim Sapag[a*]

[a.] *Laboratorio de Sólidos Porosos. Instituto de Física Aplicada. CONICET. Universidad Nacional de San Luis. Ejército de los Andes 950. CP: 5700 – San Luis. Argentina.*

[b.] *Deparment of Pharmacy and Pharmaceutical Technology, University of Granada, 18071 Granada, Spain.*

[c.] *Departamento de Química Inorgánica, Unidad Asociada al Instituto de Catálisis (CSIC), Facultad de Ciencias, Universidad de Málaga, 29071 Málaga, España.*

[d.] *Deparment of Drug Sciences, University of Pavia, viale Tatamelli 12, 22100 Pavia, Italy.*

[e.] *Andalusian Institute of Earth Sciences (Consejo Superior de Investigaciones Científicas-University of Granada) Armilla, 18100 Granada, Spain.*

Conflict of interest

There are no conflicts of interest